THE ASTROPHYSICAL JOURNAL, 451:598–606, 1995 October 1

THE DISRUPTION OF THE SAGITTARIUS DWARF GALAXY

KATHRYN V. JOHNSTON,[1] DAVID N. SPERGEL,[2] AND LARS HERNQUIST[1,3]
Received 1994 November 14; accepted 1995 April 7

ABSTRACT

Numerical simulations of dwarf spheroidal galaxies undergoing several close encounters with the Milky Way are described. By comparing our models to observed properties of the recently discovered dwarf galaxy in Sagittarius (Sgr), we discuss implications of our results for the formation and evolution of the Milky Way system. We find that existing observations are not sufficient to allow us to place precise limits on either the orbit or the initial state of the dwarf. Debris from the ongoing tidal stripping of the Sagittarius galaxy are expected to form moving groups in the halo of the Galaxy, and the discovery of such stars would strongly constrain the history and dynamical state of the dwarf. Furthermore, if Sgr is presently being disrupted, we predict that its remains will be detectable as a moving group in the halo for more than 1 Gyr. Thus, if similar accretion events have occurred in the recent history of the Galaxy, their after effects may still be observable.

Subject headings: galaxies: evolution — galaxies: individual (Sagittarius) — galaxies: interactions — galaxy: structure

1. INTRODUCTION

In 1994 April, Ibata, Gilmore, & Irwin (1994; hereafter IGI) announced the discovery of a moving group in the direction of Sagittarius, centered on the Galactic coordinates $l = 7°.5$, $b = -15°$, and which is 24 ± 2 kpc from the Sun (~ 16 kpc from the center of the Galaxy). Surface density contours of this object are elongated perpendicular to the disk of the Milky Way and are characterized by an axis ratio of $\sim 3:1$. The lowest and highest contour levels, which cover the region $l = 5°$ to $10°$, $b = -20°$ to $-10°$, span a factor of ~ 10 in surface density. The stars in the group have a heliocentric radial velocity of 153 ± 2 km s^{-1}, which corresponds to 176 km s^{-1} in Galactocentric coordinates, and a velocity dispersion of 10 km s^{-1}.

Mateo et al. (1994) subsequently obtained deep photometry of a field in this area and estimate that members of the group have typical ages of ~ 10 Gyr and metallicities of [Fe/H] $\approx -1.0 \pm 0.3$. These results, together with the lack of H I in this region (IGI), support IGI's conjecture that the moving group is a dwarf spheroidal galaxy (dSph), which would make it the ninth thus far discovered around the Milky Way. IGI compare Sgr directly to the Fornax dSph since the number of horizontal branch (HB) stars they detect ($\sim 17{,}000$) suggest that the two dwarfs are similar in size, leading to a magnitude estimate of $M_v \sim -13$ (or $L_{\rm tot} \sim 10^7\ L_\odot$) for Sgr.

Sgr's current location offers a rare opportunity to study the effects of a strong tidal interaction in detail. The tidal radii of clusters of stars of masses $10^8\ M_\odot$ and $10^7\ M_\odot$ at 16 kpc from the center of the Galaxy are 0.77 and 0.36 kpc, respectively, assuming an enclosed mass of $3 \times 10^{11}\ M_\odot$, whereas the group extends over ~ 2 kpc, which suggests that the dwarf is currently being disrupted. The extreme axis ratios inferred for Sgr are a reflection not only of the compressive shock of the encounter on the dwarf but also of the dispersal of stripped material along its orbit. Thus, the direction of Sgr's elongation traces its projected orbit.

We model the dynamics of the Milky Way and Sgr dwarf by considering encounters that are consistent with the observed properties of the group. We examine whether or not existing observations are sufficient to determine the dynamical state of the group; namely, if it is bound or unbound and whether or not it has suffered previous close encounters. Since only one component of the dwarf's velocity is known, we do not know its precise orbit and cannot hope to reproduce all observations exactly, but rather must be content to investigate the general characteristics of such encounters.

The mere existence of Sgr has implications for models of galaxy formation since the timescale for the encounter is ~ 16 kpc/176 km s^{-1} $< 10^8$ yr. Clearly, accretions of dwarf galaxies by the Milky Way must be common, or we must instead conclude that we are observing the Galaxy during a special phase of its evolution. The former possibility supports Searle & Zinn's (1978) proposal that the Galaxy was slowly built up from primordial fragments and implies that the known dSph's represent only a small fraction of a much larger original population of satellites (for reviews, see Larson 1990 and Majewski 1993a). To investigate this possibility, we follow the evolution of one simulation beyond complete tidal disruption and discuss observable consequences of such an event.

2. METHOD

2.1. *Models*

A three-component model is used for the Galaxy, in which the disk is represented by a Miyamoto & Nagai potential (1975), the spheroid by a Hernquist potential (1990a), and the halo by a logarithmic potential:

$$\Phi_{\rm disk} = -\frac{GM_{\rm disk}}{\sqrt{R^2 + (a + \sqrt{z^2 + b^2})^2}},$$

$$\Phi_{\rm spher} = -\frac{GM_{\rm spher}}{r + c},$$

$$\Phi_{\rm halo} = v_{\rm halo}^2 \ln(r^2 + d^2).$$

[1] Board of Studies in Astronomy and Astrophysics, University of California–Santa Cruz, Santa Cruz, CA 95064.
[2] Princeton University Observatory, Princeton University, Princeton, NJ 08540.
[3] Sloan Foundation Fellow, Presidential Faculty Fellow.

TABLE 1

PARAMETERS OF SIMULATIONS

Model	M	r_0	N	Orbit Type	r_{tidal}	Impulse
A.....	10^7	0.6	10^5	1	0.36	3.67
B.....	10^8	0.6	10^5	1	0.77	0.37
C.....	10^8	0.6	10^5	2	0.82	0.26
D.....	10^8	0.6	5×10^6	3	0.77	0.37

NOTE.—Length scales are in kiloparsecs, and mass is in $M_\odot$. N is the number of particles used in the simulation, and the impulse is expressed in units of the initial binding energy of the dwarf galaxy.

TABLE 2

PARAMETERS OF ORBITS

Orbit Type	Pericenter	Apocenter	Period
1	13.4	81.5	1.08
2	15.5	81.5	1.18
3	14.4	185.4	2.48

NOTE.—Length is in kiloparsecs, and time is in gigayears.

Here, $M_{disk} = 1.0 \times 10^{11}$, $M_{spher} = 3.4 \times 10^{10}$, $v_{halo} = 128$, $a = 6.5$, $b = 0.26$, $c = 0.7$, and $d = 12.0$, where masses are in $M_\odot$, velocities are in kilometers per second, and lengths are in kiloparsecs. This choice of parameters provides a nearly flat rotation curve between 1 and 30 kpc and a disk scale height of 0.2 kpc. The radial dependence of the z epicyclic frequency (κ_z) in the disk between radii at 3 and 20 kpc is similar to that of an exponential disk with a 4 kpc scale length.

Initially, the satellite is represented by a Plummer model

$$\Phi = -\frac{GM}{\sqrt{r^2 + r_0^2}},$$

where $r_0 = 0.6$ kpc and the mass is either $M = 10^7\ M_\odot$ or $M = 10^8\ M_\odot$.

For $r_0 = 0.6$ kpc, a mass of $10^7\ M_\odot$ yields a central density comparable to the luminous component of the Fornax dSph and a central velocity dispersion of 3.4 km s^{-1}, while the higher mass includes the full dynamical mass of Fornax (Mateo et al. 1993) and gives a central velocity dispersion of 10.7 km s^{-1}. Table 1 summarizes each of the simulations and provides analytic estimates of tidal radii (King 1962) and the impulsive energy input for each model on its first encounter (see Binney & Tremaine 1987). Note that model D employed 50 times as many particles as the others to permit a more detailed analysis of phase space.

Three different orbits were used in the simulations. Table 2 summarizes the properties of these orbits, and Figure 1 traces their paths. Each orbit is constrained to have a Galactocentric radial velocity of 176 km s^{-1} at a distance of 16 kpc from the center of the Galaxy and is chosen to lie in a plane perpendicular to the disk, in view of Sgr's direction of elongation. Orbits 1 and 3 illustrate the effect of varying eccentricity, assuming that Sgr has always been bound to the Milky Way, and are run in our full Galactic potential. An orbit much less eccentric than orbit 1 would lead to the complete destruction of our dwarfs in unacceptably short (<1 Gyr) timescales, while an orbit much more eccentric than orbit 3 would have an apocenter beyond the most distant observed dSphs (Leo I and Leo II). Orbit 2 is virtually identical to orbit 1 but includes the effect of only the spheroid and halo potentials so that the relative influence of the disk can be determined.

2.2. *Evolution Code*

All computations were performed on the Connection Machine 5 (CM-5) at the National Center for Supercomputing Applications (NCSA). The Milky Way is represented by a rigid potential, while the dwarf is described by a collection of self-gravitating particles whose mutual interactions are calculated using a self-consistent field code (Hernquist & Ostriker 1992). Our code has been parallelized to run on the CM-5 (Hernquist, Sigurdsson, & Bryan 1995) to maximize particle number and consequently minimize numerical relaxation (Hernquist & Barnes 1990; Weinberg 1993; Johnston & Hernquist 1995). Since the mass of the Sgr dwarf is much smaller than the mass of the Milky Way, dynamical friction and energy exchange between the parent and satellite galaxies are assumed to be negligible and have been ignored.

2.3. *Analysis*

To interpret our results, we convert the contours of the observed isopleth map of Sgr (see IGI) into mass surface densities. The lowest contour seen is at 0.125 image arcmin^{-2}, which corresponds to 0.0026 image pc^{-2} at a distance of 24 kpc, where an "image" is an HB star. This number density, n, can be related to a mass surface density using

$$\Sigma = \left(\frac{n}{0.0026}\right)\left(\frac{1}{B}\right)\left(\frac{A}{528\ L_\odot}\right)\left(\frac{C}{2.25}\right)3\ M_\odot\ \mathrm{pc}^{-2},$$

where A is the total luminosity of the system per red giant branch (RGB) star with magnitudes less then the magnitude of the HB, B is the ratio of the number of HB stars to the number of RGB stars with magnitudes less than the magnitude of the HB, and C is the mass-to-light ratio for the system. The magni-

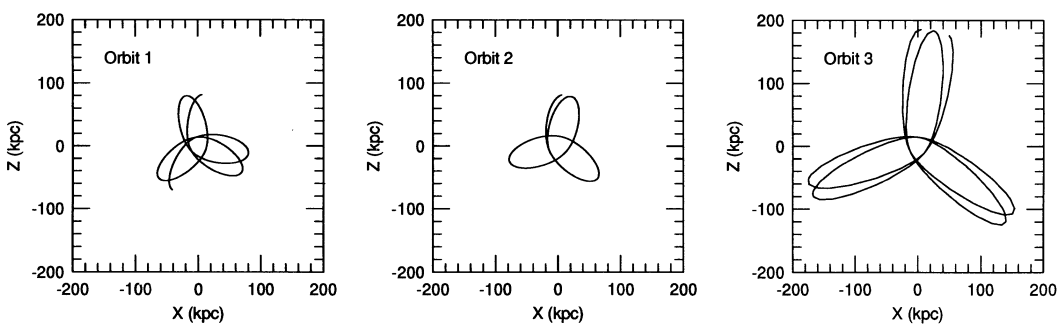

FIG. 1.—Orbits in the X-Z plane. The disk of the Milky Way lies in the X-Y plane.

tude of the HB can be approximated by

$$M_{HB} = 0.66 + 0.19[\mathrm{Fe/H}]$$

(Walker 1992), and A can be calculated from an appropriate luminosity function. Using Bergbusch & VandenBerg's (1992) isochrones for an 8.0 Gyr, [Fe/H] = −1.03 cluster, and an initial mass function exponent $x = 1.5$ gives $A = 528$. B can be estimated from observed luminosity functions and ranges from $B = 1$ to $B = 2$ for various ages and metallicities (e.g., Mighell 1990; Buonanno, Corsi, & Fusi Pesci 1985). C is 2.25 for the chosen luminosity function. Hence we estimate that $\Sigma > 1$ $M_\odot/\mathrm{pc}^2$ for the lowest contour in IGI's isopleth map.

3. RESULTS

In what follows, we first consider the effects of varying model parameters and then compare results to observations of Sgr. Figure 2, described in § 3.1, illustrates the evolution of each model. Figures 3–7, described in §§ 3.2–3.4, summarize the state of the models at times consistent with Sgr's current position and velocity relative to the Sun. Figures 8–10, described in §§ 3.5–3.7, explore the existence and persistence of moving groups in the halo.

Observations of Sgr constrain the average Galactocentric radius (16 kpc), Galactocentric radial velocity (176 km s^{-1}), and position relative to the Galactic disk (15°) of the most tightly bound particles in the simulation. To *exactly* match all these parameters on each of many passages along an orbit with a given pericenter and apocenter would require a corresponding number of simulations, with each one chosen to match the constraints on one particular passage, because the orbit is a rosette and hence the angular position of pericenter precesses. However, the halo and the disk contribute nearly equally to the disruption (see § 3.1), and the dwarf receives roughly the same energy impulse on each encounter (to within a factor of 2), irrespective of the exact orientation of the disk relative to the orbit or location of disk passage. Indeed, Figure 6, which illustrates the fifth passage of model D, shows no anomalous features when compared to the other figures, even though its most recent disk passage occurred at more than 30 kpc and the impulse from the disk was significantly smaller than in the other passages. In addition, the current position, radial velocity, and elongation of Sgr itself suggest that it is not far from its own pericenter and disk passage and is likely to have suffered from a similar impulse to that experienced by the models in our simulations. Hence, as a practical compromise, we drop the last observational constraint (orientation relative to the plane of the Galaxy) and, in Figures 3–7, consider the state of the dwarf only when it is at a radius of ∼16 kpc with a radial velocity of ∼176 km s^{-1}.

3.1. *Mass Loss and Disruption*

Figure 2 shows the fractional mass still bound by self-gravity as a function of time during each of the simulations. The curves clearly show that mass loss occurs primarily and almost instantaneously at pericenter owing to the impulsive energy input from the encounter. The orientation of the disk with respect to the orbit and the exact distance of the dwarf from the Galactic center as it passes through the disk, which both vary on each passage, do not affect the impulse significantly since the mass lost at pericenter is always of the same order.

By comparing models B and D, which differ only in their orbits, we see that the mass lost at pericenter depends weakly on orbit parameters. Model B survives fewer encounters than model D, however, because it loses mass at a greater rate throughout its (less eccentric) orbit.

Models B and C, which differ only in that the Galactic disk is excluded in model C, show substantial differences in the rate of mass loss. This result emphasizes that rather than being merely a disk-shocking phenomenon, tidal disruption involves both disk and halo shocking, the latter being much like bulge shocking of globular clusters (e.g., Aguilar, Hut, & Ostriker 1988). In fact, the internal potential energy of bound particles in model C after its fourth encounter is one-third its initial value, representing an energy gain of two-thirds its initial binding energy. Since model B, run in the full potential, was completely disrupted over the same number of encounters, we

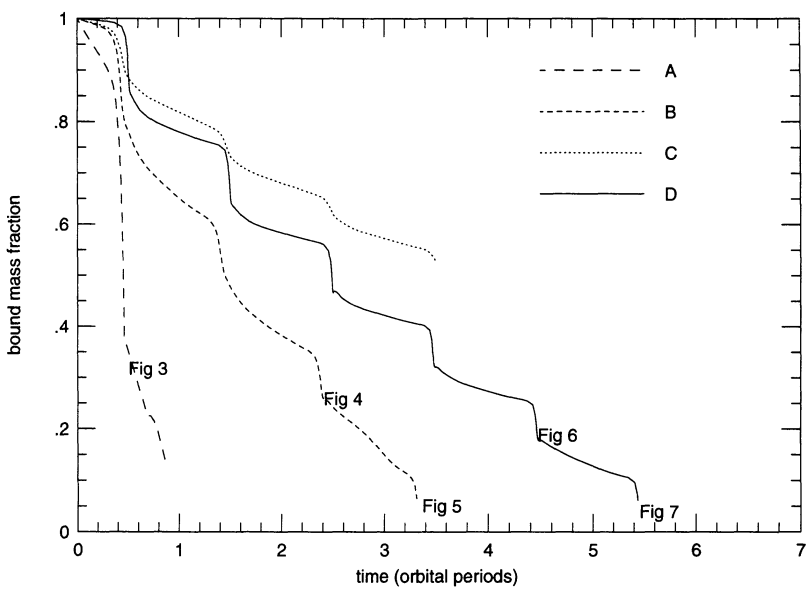

FIG. 2.—Fractional mass remaining bound as a function of time in orbital periods (T) for each simulation. The "Fig" labels show the times at which the state of a model is presented in Figs. 3–7.

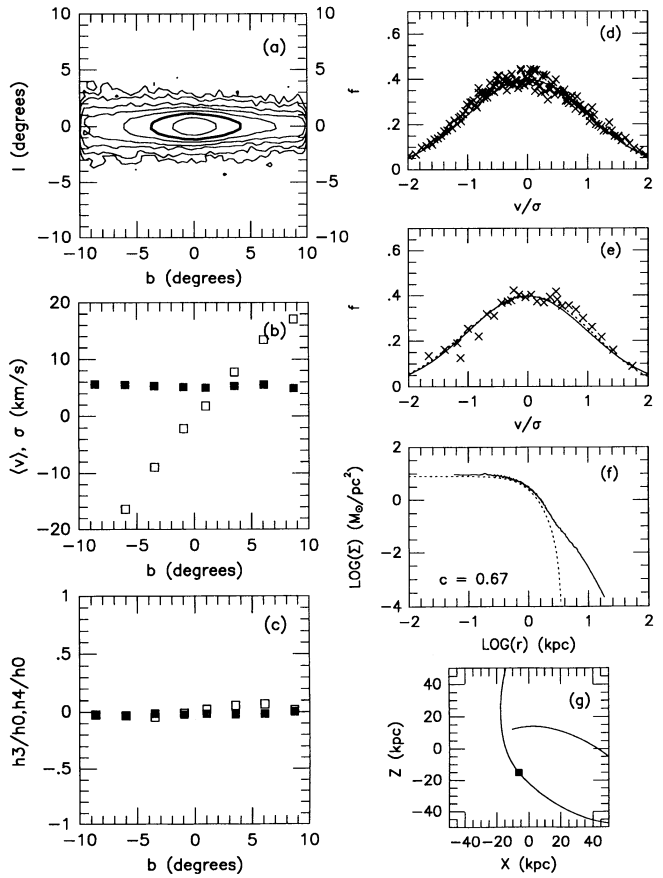

FIG. 3.— Summary of analysis at times indicated in Fig. 2. (*a*) Surface density contours. The bold contour represents 1.0 $M_\odot$ pc^{-2}. Consecutive contours are a factor of $(10)^{1/2}$ apart. (*b*) Line-of-sight average velocity (*open symbols*) and velocity dispersion (*closed symbols*) along the projected major axis. (*c*) Normalized Gauss-Hermite moments (*see text*). (*d*) Line-of-sight velocity distribution of particles in the bin at $-1°$ (used in *b* and *c*; *f* is the fraction of particles per unit σ). The solid line is a Gaussian of the same velocity dispersion. The dotted line includes the higher Gauss-Hermite moments. The crosses indicate the points from simple binning of the data. (*e*) Same as (*d*), but for the $-9°$ bin. (*f*) Surface density profile (*solid line*). For comparison, a King model of the given concentration [$c = \log(r_{tidal}/r_{core})$] is shown by the dotted line. (*g*) Point along orbit at which the analysis was done.

infer that the last one-third of its binding energy must have been gained from the disk. We conclude that at least half of the energy gained from the encounters in the full potential comes from halo shocking alone. In addition, from the distorted shape of its surface density contours it is impossible to infer if Sgr has yet passed through the disk since the disk is not solely responsible for the satellite's destruction.

3.2. *Surface Densities*

In Figures 3–7 we present results from the viewpoint of an observer at rest with respect to the center of the Galaxy and 24 kpc from the dwarf on the opposite side of the bulge.

Panel *a* of each figure shows mass surface density contours, with the bold contour at the level 1 $M_\odot$/pc^2. The isopleths of the observed star counts are much less smooth than the contours in our figures, probably due to uncertainties in the counts themselves and because of dust obscuration toward the bulge of the Galaxy. However, each simulated map compares well in extent, ellipticity, density contrast, and absolute density to the observations.

Panel *f* of each figure shows the surface density profile calculated on concentric ellipses, with an ellipticity chosen to fit the contour at 5° along the major axis (*solid line*). The dotted line is a King model of the given concentration, plotted for comparison. The central surface density and concentration parameter of the King model fitted to the profiles both decrease with increasing number of pericentric passages until a critical point is reached, after which full disruption occurs. On the last passage prior to disruption, all our models (irrespective of orbit and initial conditions) are well fitted by nearly identical King models. This interesting coincidence merits further investigation but is not something we discuss further here. A fuller exploration of parameter space (varying both the mass and the scale length of the initial model) would be necessary to address this issue since the criterion for tidal disruption involves the density contrast of the satellite and parent galaxies. (Previous numerical investigations of tidal interactions and density criteria for disruption include Miller 1986; McGlynn 1990; and Oh, Lin, & Aarseth 1995.)

3.3. *Kinematics*

For the kinematic analyses all velocities are projected along the line of sight noted in the previous section. Particles are ordered by their position along the major axis (positive angles are in the direction of motion of the dwarf) and then binned into eight $(1\overset{\circ}{.}25)^2$ boxes before calculating the velocity moments. No bin contains fewer than 100 particles.

Panel *b* of each figure shows the average velocity (*open symbols*) and velocity dispersion (*filled symbols*) of particles in

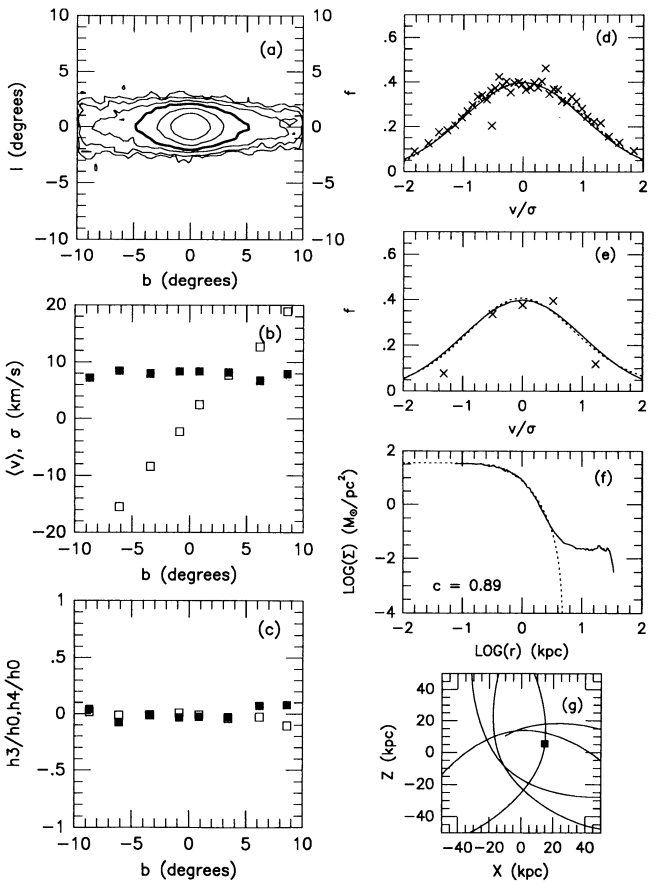

FIG. 4.—Same as Fig. 3

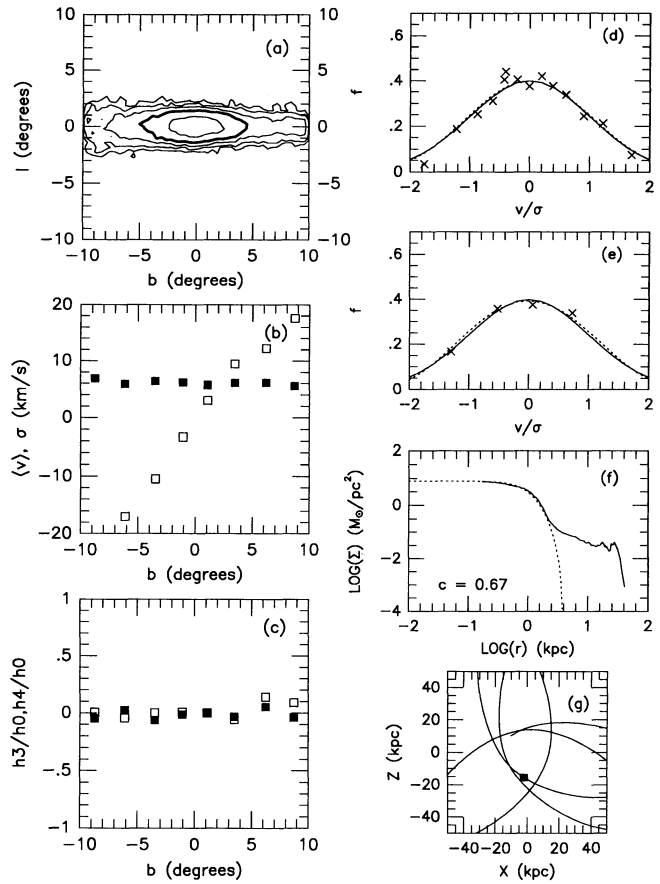

FIG. 5.—Same as Fig. 3

bins along the major axis of the contour map. It is interesting to note that tidal stripping does not enhance the line-of-sight velocity dispersion, even out to projected distances of 10°.

The models have a substantial positive velocity gradient (>2 km s^{-1} deg^{-1}) along their major axes. Two effects contribute to line-of-sight velocity gradients observed along the projected major axis of a satellite in the tidal field of the Milky Way. The first is due to the combination of the tangential velocity, v_t, of the satellite with its angular extent on the sky. An angular separation of $\Delta\theta$ between two lines of sight along the major axis leads to a velocity difference of $v_t \sin \Delta\theta$ (assuming that the major axis is coincident with the tangential velocity vector). The second is due to stripping of material from the satellite. Stars forming the leading streamer are pulled toward the Galaxy to lower energy orbits, and those forming the trailing streamer are pulled away to higher energy orbits (Oh et al. 1995). Clearly the sign and magnitude of the gradient will depend on the position of the observer relative to the Galactocentric radius vector of the satellite and the strength of the tidal interaction. In our case (for a line of sight coincident with the radius vector), the first effect leads to a positive velocity gradient in the direction of motion of the satellite, while the second leads to a negative gradient. In Figures 3–7 the dwarf has a large angular extent on the sky and the first effect dominates, with model D (Figs. 6 and 7) showing the most significant gradient because it is on a higher energy orbit and has a larger v_t.

Panel *c* of each figure shows normalized values of the Gauss-Hermite moments calculated for particles in each bin. These moments quantify the deviation of the velocity distribution from a Gaussian (Gerhard 1993; van der Marel & Franx 1993). We have chosen van der Marel & Franx's formalism using the derivation outlined in Heyl, Hernquist, & Spergel (1995). Since the higher order moments are only a few percent of the zeroth-order term, the distribution is nearly Gaussian along the major axis, as confirmed in panels *d* and *e* of each figure, which show the velocity distribution of particles in the bins at $-9°$ and $-1°$, respectively.

3.4. *Comparison with Observations*

There are no striking differences between Figures 3–7, and each contour map (panel *a*) and velocity dispersion profile (panel *b*) compares well with the results reported in IGI (see §§ 3.2 and 3.3). Hence we cannot constrain the initial mass of the dwarf or its orbit using these observed quantities alone. In addition, it is hard to distinguish between a passage in which a bound core of particles still remains, as in Figures 4 and 6, from one in which all particles are unbound, as in Figures 5 and 7, and thus Sgr is neither necessarily on its first nor on its last pericentric passage.

An accurate determination of Sgr's velocity profile would provide a stronger constraint on its history (see § 3.3). Indeed, based on the low velocity difference along its major axis reported in IGI (<1 km s^{-1} deg^{-1}), Velázquez & White (1995) predict an orbit for Sgr which has a much shorter period (0.76 Gyr) than the ones we explored. However, a dwarf spheroidal in such a tightly bound orbit would not survive long, and it seems difficult to reconcile the 10 Gyr stellar ages inferred by

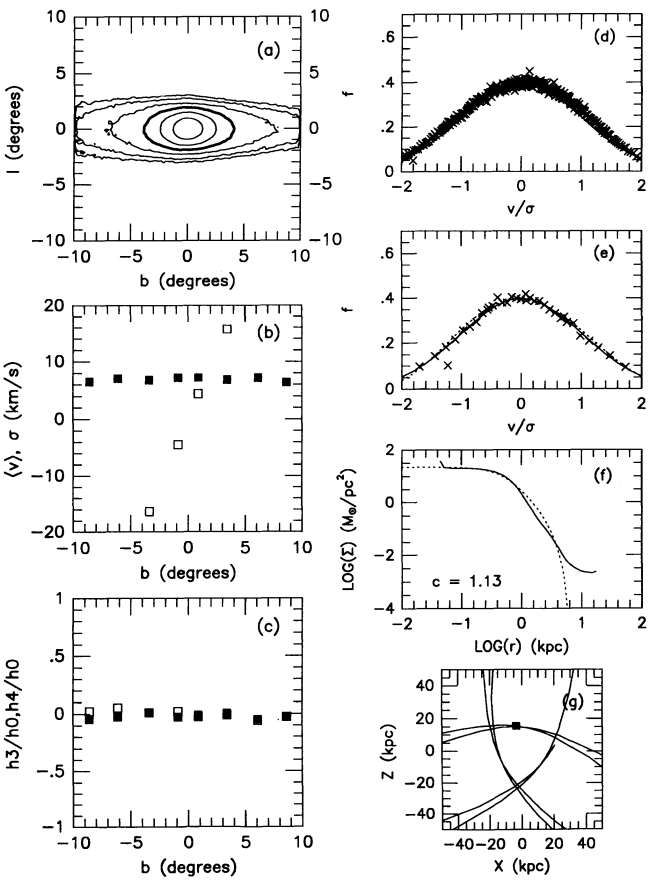

FIG. 6.—Same as Fig. 3

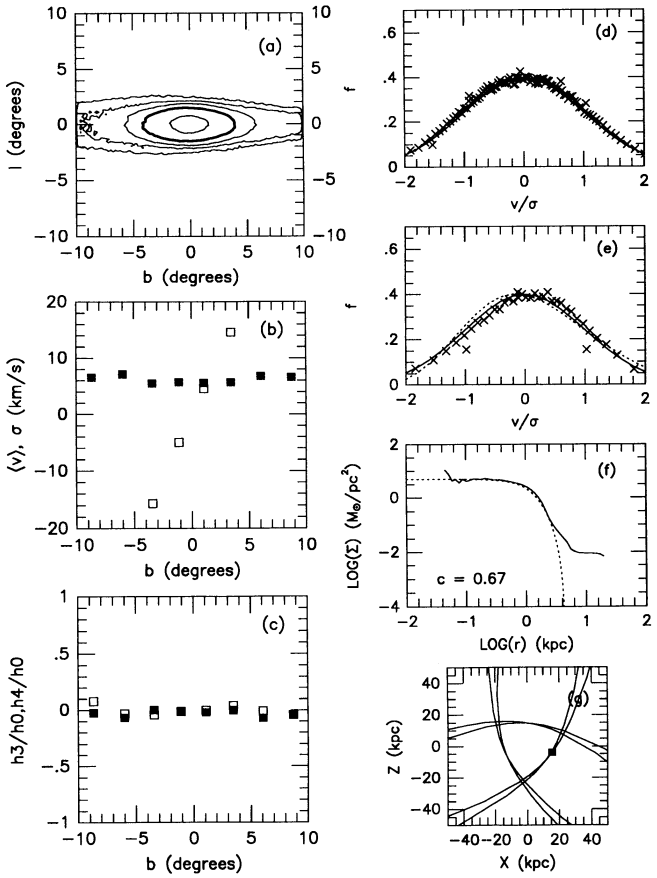

FIG. 7.—Same as Fig. 3

Mateo et al. (1994) with a short disruption timescale. Moreover, recent observations (Ibata et al. 1995) have found a gradient increasing to 3 km s^{-1} deg^{-1} at $b = -25°$ (which is equivalent to $b = -10°$ in our figures). This in turn compares well with our models, which all have substantial velocity gradients of 2–4 km s^{-1} deg^{-1}. Further observations are needed to conclusively distinguish between these different scenarios.

3.5. *Phase Space Structure*

For the remainder of § 3 we discuss the position-velocity phase space evolution of model D in detail. This model employed 50 times as many particles as the others to improve resolution and accuracy. In addition, this was the only model with a disruption timescale of order the Hubble time.

Figure 8 shows the radial velocity as a function of radius for a sample of 2500 particles immediately following the final passage of the satellite (at the time illustrated in Fig. 7). The solid line traces the dwarf's orbit. At this time the model has undergone six pericentric passages over the course of 13 Gyr, and it has been fully disrupted. Each encounter has produced its own distinct tidal streamer. Nevertheless, the particles occupy a relatively small region of phase space. We hope to exploit this high density to locate tidal debris from cannibalized dwarfs in the halo of our Galaxy.

3.6. *Streamers as Moving Groups*

The Sagittarius dwarf was first recognized as a moving group. Is it possible to detect the streamers from the encounter away from the Galactic center? In Figure 9, we examine the line-of-sight velocity distributions of stars in two different square-degree regions. The viewpoint is again that of an observer at rest with respect to the center of the Galaxy and 24 kpc

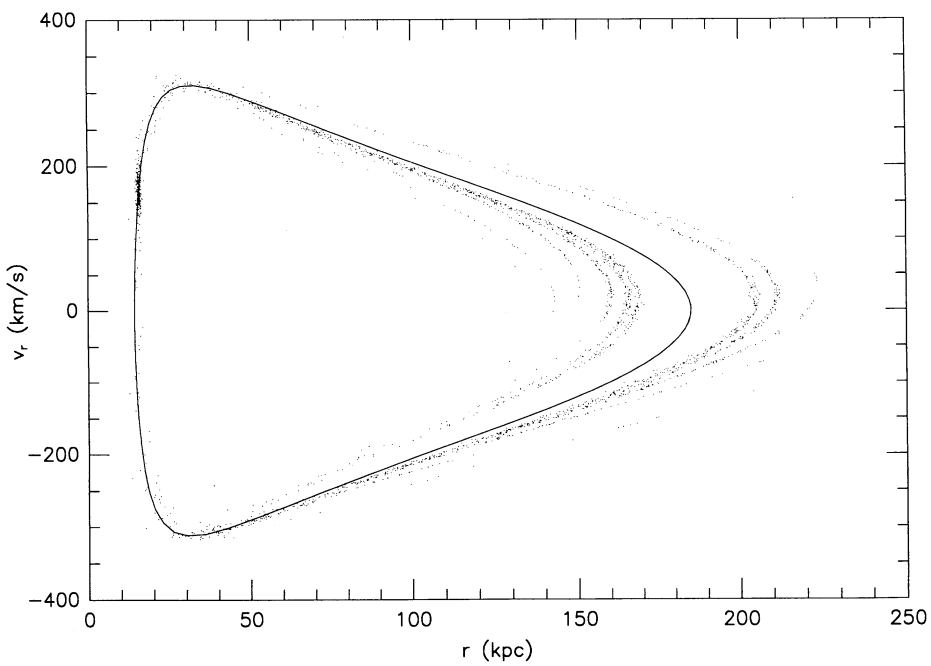

FIG. 8.—Galactocentric radial velocity vs. radius for random sample of 2500 particles. The solid line is the locus of the orbit in this plane.

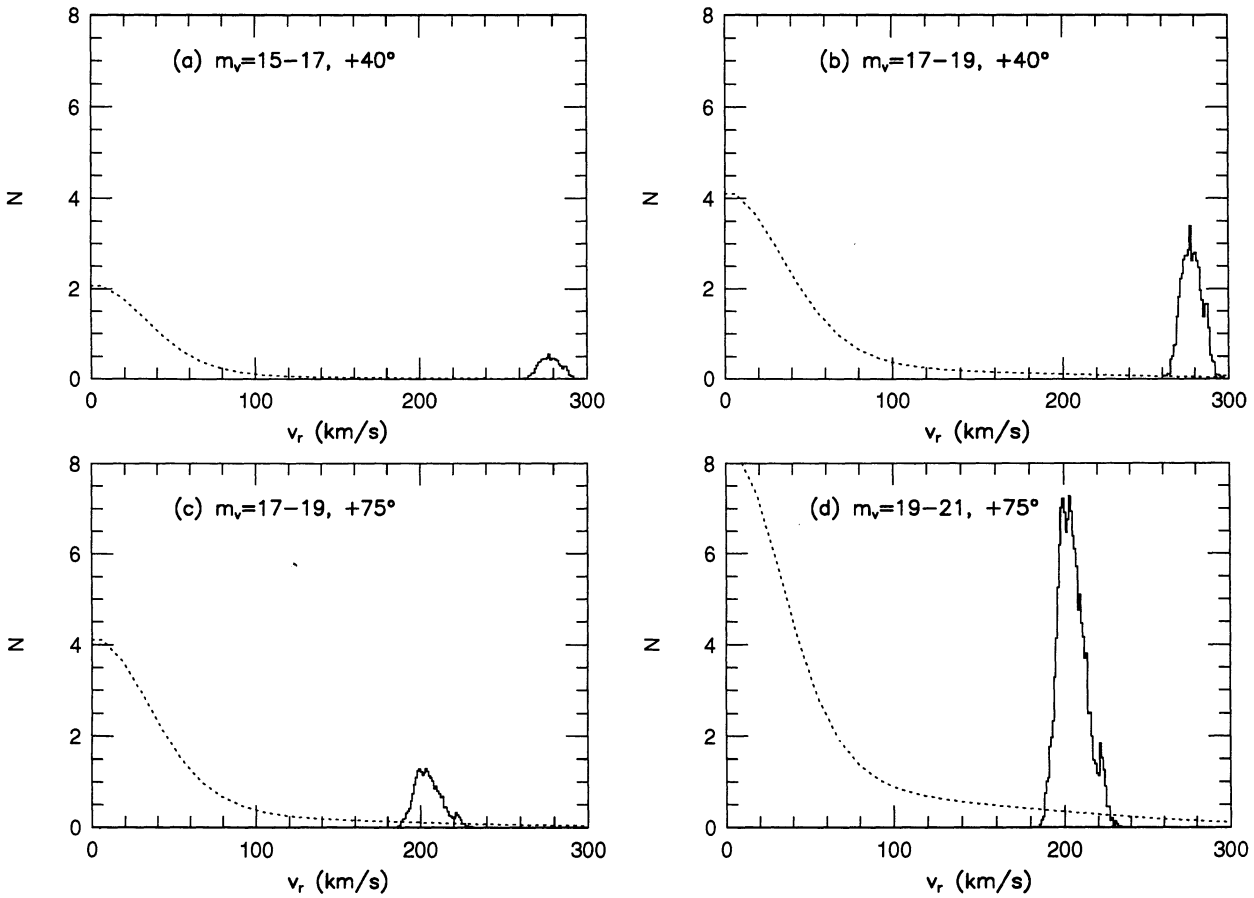

FIG. 9.—Analysis of tidal streamers. N is the number of stars per (degree)^2 per 1 km s^{-1} bin at 40° (*a* and *b*) and 75° (*c* and *d*) from the dwarf. The dotted line shows the background toward the north Galactic pole. The solid line is from the simulation. The different panels are for the stated magnitude bins.

from the dwarf on the opposite side of the bulge. Panels *a* and *b* are for stars 40° away from the dwarf along its orbit, while panels *c* and *d* show similar information at 75°. Apparent magnitudes are estimated using the adopted luminosity function (*solid line*). Also plotted in each of the panels is an estimate of the observed numbers of stars as a function of line-of-sight velocity in these directions (*dotted line*). These distributions were generated using the star counts of thin disk, thick disk, and halo stars in the direction of the north Galactic pole (Reid & Majewski 1993). The velocity distribution of each component is modeled as a Maxwellian with z-velocity dispersions of 30, 45, and 150 km s^{-1} for the three components, respectively. A comparison of the areas under the two curves in each panel shows that the surface density of the stars in the streamers is only ~10% of the background. However, the tidal streamers stand out as moving groups in all magnitude bins, although the exact distribution depends on the details of the encounter. Observing such a group directly associated with the Sagittarius dwarf would strongly constrain its orbit and hence its history. The tidal streamers are expected to trace the great circle defined by Sgr's elongation.

For model D's orbit, however, it seems unlikely that the streamers could also be observed as moving groups in proper motion studies. The square-degree surveyed at 40° contains particles at ~37 kpc with tangential velocities of ~370 km s^{-1}, which corresponds to a proper motion of 2.2×10^{-3} arcsec yr^{-1}, well below the current observational limits for such surveys.

3.7. *Moving Groups Following Disruption*

In Figure 10 we consider the persistence of moving groups in the halo, following model D beyond its complete destruction on its sixth pericentric passage. The model maintains a "core" of unbound stars at densities higher than the tidal streamers for more than 1 Gyr after this passage. This "core" could not be confused with a dwarf spheroidal galaxy, however, since its surface density quickly falls below 0.1 $M_\odot$pc^{-2}, an order of magnitude smaller than that of the Galaxy's satellites (Mateo et al. 1993). The persistence of this "core" does not contradict estimates of the timescale for the dwarf to disperse following its disruption [$\sim r_0/\sigma \sim$ (500 pc)/(10 km s^{-1}) ~ 10^8 yr]. At 1 Gyr after disruption, the dwarf's surface density has already fallen by a factor of 10 because of the free streaming of the higher velocity stars away from the region. The remaining "core" consists of the lowest velocity stars whose dispersion is much less than 10 km s^{-1} and, hence, whose dispersion timescale is much longer than 10^8 yr.

Figures 10*a*–10*b* show the velocity distribution of stars in the "core" in two different magnitude bins, 0.5 Gyr after pericenter. Figure 10*c* is a similar plot, 1 Gyr after pericenter. All three suggest that such a group could be observed. Figure 10*d* is the velocity distribution of stars 10° further along the orbit

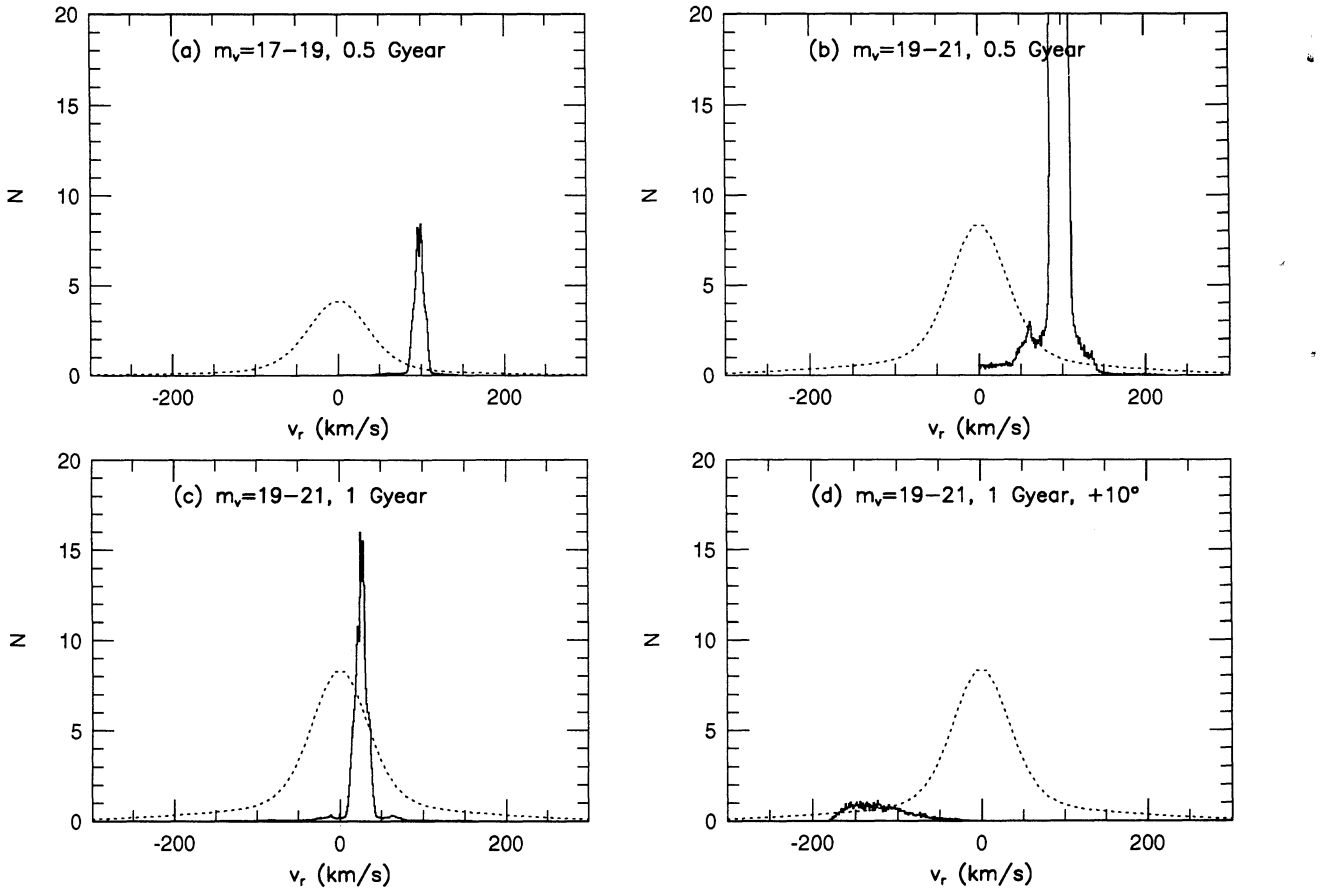

FIG. 10.—Same as Fig. 9, but for the dwarf at 0.5 Gyr (*a* and *b*) and 1.0 Gyr (*c* and *d*) after disruption

than those in Figure 10*c*, and here the moving group is not so obvious. Note, however, that these stars are more than 160 kpc away from the center of the Galaxy. Presumably, it would be less challenging to detect a disrupting dwarf on a more tightly bound orbit.

3.8. *Carbon Stars and Globular Clusters*

The Fornax dSph contains ~65 carbon stars (Richer & Westerlund 1983) and five globular clusters (Hodge 1988). The disruption of such a system might leave some signatures of the event, such as substructure in the halo carbon star and globular cluster populations. Indeed, IGI report the existence of four globular clusters in the vicinity of Sgr itself.

In the previous section, the square degree examined in Figure 10*a* contains ~5% of the initial mass of the model. For a Fornax-like population, such a region would contain about three high-velocity carbon stars, giving a surface density significantly higher than the average (0.02 deg^{-2}) estimated to a depth of $M_v = 18$ for faint, high-latitude carbon stars by Green et al. (1994).

Clearly, the strategy of identifying debris by its overdensity in a small region of phase-space would not work for globular clusters from disrupted dwarfs. However, the satellite galaxies of the Milky Way tend to lie in the great circles defined by the Magellanic Stream (the Magellanic Plane) and the Fornax-Leo-Sculptor stream, as noted first by Lynden-Bell (1976, 1982). Globular clusters have subsequently been associated with both these planes (Lin & Richer 1992; Majewski 1994). These great circles present obvious targets to search for moving groups, and their discovery would be further proof that the alignment of halo objects is not mere coincidence, but rather the signature of tidal interactions and accretions of satellites by the Milky Way.

4. DISCUSSION

Five main conclusions follow from our work:

1. For pericenters of $\gtrsim 13$ kpc, the contribution of the halo to the disruption of a dwarf spheroidal of mass less than 10^8 $M_\odot$ is at least that of the disk.
2. The dwarf galaxy in Sagittarius is neither necessarily on its first nor on its last Galactic passage, despite tidal radius arguments.
3. It is not possible to distinguish among a wide range of orbital parameters and initial dwarf models using the observed surface density distribution alone. It is also not possible to determine the direction of motion of Sgr from its distorted state, and so we cannot say if we are currently observing it immediately prior to or following disk passage.
4. Debris from the dwarf's most recent passage should be observable as moving groups in the halo.
5. It may be possible to infer whether or not similar events have occurred within the past 10^9 yr from observations of moving groups in the halo.

Conclusion 1 has implications for models of Galaxy formation. The existence of the thin disk is often used as evidence

against substantial recent accretion of satellites by the Galaxy (e.g., Tóth & Ostriker 1992; Quinn, Hernquist, & Fullagar 1993, and references therein). In our simulations, if half of the initial binding energy of a $10^8\ M_\odot$ satellite is converted entirely into random energy in a $10^{11}\ M_\odot$ disk, this would increase the z-velocity dispersion (σ_z) in the disk by only ~ 0.25 km s^{-1}. Moreover, the important contribution of the halo to tidal disruption implies that dwarfs could easily be destroyed on orbits with larger pericenters by halo shocking alone, with negligible effect on the disk.

These findings are consistent with earlier studies which stress the fragility of disks (Quinn & Goodman 1986; Quinn et al. 1993; Walker, Mihos, & Hernquist 1995). In the simulations of Walker et al. (1995), for example, the satellite orbit decays quickly both radially and into the plane of the disk through dynamical friction with the disk and the halo. A substantial fraction of both the orbital and internal energy of the satellite is lost to the disk and σ_z can increase significantly through a single accretion event. In our calculations, the ratio of satellite mass to disk mass is an order of magnitude smaller than previous studies. Since frictional deceleration is proportional to the mass of the satellite ($M_{\rm sat}$), the timescale for orbital decay ($\propto 1/M_{\rm sat}$) is much longer (see Binney & Tremaine 1987). More of the orbital energy is carried away by stripped particles, and less is deposited in the disk. Hence, our estimate of an increase of 0.25 km s^{-1} in σ_z suggests that the Galaxy could absorb 10^9–$10^{10}\ M_\odot$ in small accretion events and still maintain a thin disk. This supports Searle & Zinn's view of the formation of the Milky Way from primordial fragments. (For further discussion, see, e.g., Hernquist 1990b; Hernquist & Quinn 1993; and Majewski 1993b.) However, fully self-consistent simulations are needed to precisely determine the relative importance of the disk and halo to the orbital decay and disruption of small satellites.

Conclusions 4 and 5 emphasize the value of observational kinematic studies. A number of moving groups have already been reported in the literature (see Preston, Beers, & Shectman 1994; Majewski, Munn, & Hawley 1994, and references therein). The discovery of moving groups in the halo associated with Sgr would constrain its orbit, origin, and history. Observations of such groups in general (or limits on their occurrence) would tell us something about the frequency of accretion events in the recent history of our Galaxy. A smooth phase-space distribution argues in favor of a relatively uneventful past, while a nonuniform one points to the more common occurrence of dwarf galaxy accretion, much as we are witnessing today in Sgr.

Since we do not know the history of the Galaxy, we cannot rely on surveys covering only a few square arcminutes (e.g., Bahcall et al. 1994) to tell us much beyond the local properties of the region observed. If the halo was indeed formed from many accretion events, we would expect nonuniformity on square-degree scales because of this history, and it would only be through a survey covering many square degrees on the sky that we could obtain global estimates of its content and structure

We thank Mike Bolte for many helpful comments and Doug Lin, Mike Irwin, Neil Tyson, and Burt Jones for useful discussion. This work was supported in part by the National Center for Supercomputing Applications, the Alfred P. Sloan Foundation, NASA Theory Grant NAGW-2422, NSF Grants 90-18526, ASC 93-18185 and AST 91-17388, and the Presidential Faculty Fellows program.

REFERENCES

Aguilar, L., Hut, P., & Ostriker, J. P. 1988, ApJ, 335, 720
Bahcall, J. N., Flynn, C., Gould, A., & Kirhakos, S. 1994, preprint
Bergbusch, P. A., & VandenBerg, D. A. 1992, ApJS, 81,163
Binney, J., & Tremaine, S. 1987, Galactic Dynamics (Princeton: Princeton Univ. Press)
Buonanno, R., Corsi, C. E., & Fusi Pecci, F. 1985, A&A, 145, 97
Gerhard, O. E. 1993, MNRAS, 265, 213
Green, P. J., Margon, B., Anderson, S. F., & Cook, K. H. 1994, ApJ, 434, 319
Hernquist, L. 1990a, ApJ, 356, 359
———. 1990b, in Warped Disks and Inclined Rings around Galaxies, ed. S. Casertano, P. Sackett, & F. Briggs (Cambridge: Cambridge Univ. Press), 96
Hernquist, L., & Barnes, J. E. 1990, ApJ, 349, 562
Hernquist, L., & Ostriker, J. P. 1992, ApJ, 386, 375
Hernquist, L., & Quinn, P. J. 1993, in Galaxy Evolution: the Milky Way Perspective, ed. S. R. Majewski (San Francisco: ASP), 187
Hernquist, L., Sigurdsson, S., & Bryan, G. 1995, ApJ, 446, 717
Heyl, J., Hernquist, L., & Spergel, D. N. 1995, ApJ, 448, 64
Hodge, P. 1988 PASP, 100, 568
Ibata, R. A., Gilmore, G., & Irwin, M. J. 1994, Nature, 370, 194 (IGI)
Ibata, R. A., Irwin, M. J., Gilmore, G., & Suntzeff, N. B. 1995, private communication
Johnston, K. V., & Hernquist, L. 1995, in preparation
King, I. R. 1962, AJ, 67, 471
Larson, R. B. 1990, PASP, 102, 709
Lin, D. N. C., & Richer, H. B. 1992, ApJ, 388, L57
Lynden-Bell, D. 1976, MNRAS, 174, 695
———. 1982, Observatory, 102, 202
Majewski, S. R. 1993a, ARA&A, 31, 575
———. 1993b, in Galaxy Evolution: the Milky Way Perspective, ed. S. R. Majewski (San Francisco: ASP), 5
———. 1994, ApJ, 431, L17
Majewski, S. R., Munn, J. A., & Hawley, S. L. 1994, ApJ, 427, L37
Mateo, M., Olszewski, E. W., Pryor, C., Welch, D. L., & Fischer, P. 1993, AJ, 105, 510
Mateo, M., Udalski, A., Szymański, M., Kałżuny, J., Kubiak, M., & Krzeminski, W. 1994, preprin
McGlynn, T. A. 1990, ApJ, 348, 515
Mighell, K. 1990, A&AS, 82, 207
Miller, R. H. 1986, A&A, 167, 41
Miyamoto, M., & Nagai, R. 1975, PASJ, 27, 533
Oh, K. S., Lin, D. N. C., & Aarseth, S. J. 1995, ApJ, 442, 142
Preston, G. W., Beers, T. C., & Shectman, S. A. 1994, AJ, 108, 538
Quinn, P. J., & Goodman, J. 1986, ApJ, 309, 472
Quinn, P. J., Hernquist, L., & Fullagar, D. P. 1993, ApJ, 403, 74
Reid, N., & Majewski, S. R. 1993, ApJ, 409, 635
Richer, H. B., & Westerlund, B. E. 1983 ApJ, 264, 114
Searle, L., & Zinn, R. 1978, ApJ, 225, 357
Tóth, G., & Ostriker, J. P. 1992, ApJ, 389, 5
van der Marel, R. P., & Franx, M. 1993, ApJ, 407, 525.
Velázquez, H., & White, S. D. M. 1995, preprint
Walker, A. R. 1992, ApJ, 390, L81
Walker, I., Mihos, J. C., & Hernquist, L. 1995, ApJ, submitted
Weinberg, M. 1993, ApJ, 410, 543